Deactivation of a steam reformer catalyst in chemical looping hydrogen systems: experiments and modeling

IOP Publishing J. Phys. Energy 5 (2023) 014021 https://doi.org/10.1088/2515-7655/acb668

Journal of Physics: Energy

OPEN ACCESS

RECEIVED
8 September 2022

REVISED
13 January 2023

ACCEPTED FOR PUBLICATION
26 January 2023

PUBLISHED
9 February 2023

PAPER

Deactivation of a steam reformer catalyst in chemical looping hydrogen systems: experiments and modeling

B Stoppacher[1,*], F Lonardi[2], S Bock[1], M Bele[3], A Bertucco[2] and V Hacker[1]

[1] Institute of Chemical Engineering and Environmental Technology, Graz University of Technology, Inffeldgasse 25/C, 8010 Graz, Austria
[2] Department of Industrial Engineering, University of Padua, Via F. Marzolo 9, 35131 Padova, Italy
[3] Department of Materials Chemistry, National Institute of Chemistry, Hajdrihova 19, Ljubljana 1001, Slovenia
[*] Author to whom any correspondence should be addressed.

E-mail: bernd.stoppacher@tugraz.at

Keywords: chemical looping hydrogen, biogas reforming, catalyst deactivation, kinetic modeling

Supplementary material for this article is available online

Abstract

The utilization of real producer gases such as raw biogas or gasified wood for chemical looping hydrogen production implies the introduction of harmful contaminants into the process. Hydrogen sulfide represents one of the most challenging trace gases in the reformer steam iron cycle. The aim of the present work was an in-depth investigation of steam reforming with pure methane and synthetic biogas contaminated with selective concentrations of 1, 5 and 10 ppm of hydrogen sulfide. To validate the experimental data, the fixed-bed reactor system was modeled as one-dimensional pseudo-homogeneous plug flow reactor by an adapted Maxted model. In a preliminary thermodynamic study, the dry equilibrium composition was determined within a deviation of 4% for steam methane reforming (SMR) and 2% for synthetic biogas reforming compared to the experimental results. The impact of hydrogen sulfide on the reactivity of the catalyst was characterized by the residual methane conversion. The deactivation rate and extent is directly proportional to the concentration of H_2S, as higher hydrogen sulfide concentrations lead to a faster deactivation and lower residual methane conversion. A comparison of the methane conversion as a function of sulfur coverage between experimental and simulated data showed good agreement. The predicted results are within $<10\%$ deviation for SMR and synthetic biogas reforming, except for sulfur coverages between 0.6 and 0.8. The temperature in the catalyst bed was monitored throughout the deactivation process to gather additional information about the reaction behavior. It was possible to visualize the shift of the reforming reaction front towards the bottom of the reactor caused by catalyst deactivation. The impact of sulfur chemisorption on the morphology of the steam reformer catalyst was analyzed by scanning electron microscope (SEM/EDS) and Brunnauer–Emmet–Teller techniques. SEM patterns clearly indicated the presence of sulfur as a sort of dust on the surface of the catalyst, which was confirmed by EDS analysis with a sulfur concentration of 0.04 wt%.

Nomenclature

SRB	Sulfate reducing bacteria
RESC	Reformer steam iron cycle
NET	Negative emission technology
SEM	Scanning electron microscope
EDS	Energy dispersive x-ray spectroscopy
XRD	X-ray diffraction
BET	Brunnauer–Emmet–Teller
CCS	Carbon capture and storage
CLC	Chemical looping combustion
CLOU	Chemical looping oxygen uncoupling
CLH	Chemical looping hydrogen
μGC	Micro-gas chromatograph
S/C	Steam to carbon ratio (-)
O/R	Oxidative to reductive compounds ratio (-)
SMR	Steam methane reforming
WGS	Water gas shift reaction
RM	Reverse methanation
DEN	Denominator
a, b	Constant parameters
MM	Molar mass
HPLC	High pressure liquid chromatography
PTFE	Polytetrafluoroethylene
$\Delta H_{R,298}$	Molar heat of reaction (kJ mol^{-1})
$\dot{n}$	Molar flow (mol min^{-1})
$\dot{V}$	Volume flow (Nl min^{-1})
V	Volume (Nl)
m	Mass (g)
t	Time (min)
y	Volume fraction (-)
R	Reaction rate
T	Temperature (K)
p	Pressure (bar)
$\hat{A}$	Pellet specific surface area (m^2 g^{-1})
h	Pellet heat transfer coefficient (kJ h^{-1} m K^{-1})
c_p	Molar heat capacity (kJ g^{-1} K^{-1})
Q	Heat transfer rate (kW)
k	Reaction rate constant
Kp	Reaction equilibrium constant
K	Adsorption equilibrium constant
Ea	Activation energy (kJ mol^{-1})
S	Entropy (kJ K^{-1})
$\hat{S}$	Nickel surface area (m^2 g^{-1})

Greek symbols

ν	Stoichiometric coefficient
η	Effectiveness factor (-)
Σ	Sum
Θ	Coverage (-)

Subscripts

i, j, k	Continuous variables
m	Molar
tot	Total
S	Sulfur
C	Carbon
cat	Catalyst
f	Furnace
R	Reaction
max	Maximum
exp	Experimental
for	Forward
back	Backward

Superscripts

acc	Accumulated
·	Flow

1. Introduction

The global energy supply from fossil fuels was responsible for more than 400 Mt of CO_2 emissions in 2021 and is thus a major contributor to global warming [1]. The substitution of fossil fuels with green hydrogen is a promising way for the decarbonization of the current energy system. Locally available, renewable primary energy carriers such as biomass, biogenic waste or sewage sludge have been suggested as CO_2-free alternative feedstocks for decentralized hydrogen production. In addition, the large dependency on fossil fuels can be reduced. Biogas is produced by anaerobic digestion of biogenic matter like energy crops, agriculture residues or municipal solid waste. In general, three types of anaerobic bacteria convert carbohydrates, proteins and lipids by hydrolysis to sugars, amino acids and fatty acids. Acidogenesis, acetogenesis and methanogenesis reactions eventually produce methane and carbon dioxide. Beside these reactions, hydrogen sulfide is formed from organically bounded sulfur present in proteins or from SO_4^- by SRB. It can enrich in biogas up to a concentration of 5400 ppm depending on the type and composition of the feedstock [2, 3].

It is well known that hydrogen sulfide deactivate Ni-based reformer catalysts even at trace gas levels [4–7]. According to Argyle and Bartholomew [8], sulfur poisoning is the main threat to the reformer catalyst activity apart from fouling by carbon. It occurs through the favored chemisorption of sulfur atoms present in impurities, products or reactants on actives sites that would otherwise be available for the favored reaction. This phenomenon is caused by the higher adsorption strength of sulfur compared to the favored reactant. Consequently, at least three to four topside sites of the catalyst are physically blocked. Moreover, the electrical modification of neighbor atoms causes a lower adsorption ability of the favored reactants [9].

Chemical looping processes enable the production of high-purity hydrogen from various carbonaceous feedstock such as natural gas, biogas, gasified biomass, bio-alcohols and more. Based on the ability of metal oxides to oxidize gaseous and solid fuels, high-purity product gas streams can be produced. In the first process step, metal oxides are reduced to metals or a metal oxide of lower oxidation state. As product gas, pure carbon dioxide is released what enables CCS. The final re-oxidation of the metal with e.g. air as an oxidizer allows the spatial or temporal separation of the oxidizing and reducing gas stream. This principle can be adopted for hydrogen production, substituting air with steam as the oxidation medium. At first, a suitable synthesis gas is produced by gasification of biomass or through steam-methane reforming (see equations (1) and (2)). The syngas then reduces an iron-based oxygen carrier (equations (3)–(5)). In the oxidation step, iron is re-oxidized to magnetite by steam and high purity hydrogen is released (equations (6)–(7)). To reach the original oxidation state of the used iron oxide, an additional air oxidation step is performed (equation (8)):

$$C_xH_y + H_2O \leftrightarrow xCO + yH_2 \qquad \Delta H_{R,298} = +247.0\ \text{kJ mol}^{-1} \tag{1}$$

$$CO + H_2O \leftrightarrow CO_2 + H_2 \qquad \Delta H_{R,298} = -41.1\ \text{kJ mol}^{-1} \tag{2}$$

$$3Fe_2O_3 + H_2/CO \leftrightarrow 2Fe_3O_4 + H_2O/CO_2 \qquad \Delta H_{R,298} = -43.3/-40.4\ \text{kJ mol}^{-1} \tag{3}$$

$$Fe_3O_4 + H_2/CO \leftrightarrow 3FeO + \frac{H_2O}{CO_2} \qquad \Delta H_{R,298} = +74.7/+33.6\ \text{kJ mol}^{-1} \tag{4}$$

$$FeO + H_2/CO \leftrightarrow Fe + H_2O/CO_2 \qquad \Delta H_{R,298} = +25.4/-15.7\ \text{kJ mol}^{-1} \tag{5}$$

$$3Fe + 4H_2O \leftrightarrow Fe_3O_4 + 4H_2 \qquad \Delta H_{R,298} = -151.1\ \text{kJ mol}^{-1} \tag{6}$$

$$3FeO + H_2O \leftrightarrow Fe_3O_4 + H_2 \qquad \Delta H_{R,298} = -74.7\ \text{kJ mol}^{-1} \tag{7}$$

$$4Fe_3O_4 + O_2 \leftrightarrow 6Fe_2O_3 \qquad \Delta H_{R,298} = -485.1\ \text{kJ mol}^{-1}. \tag{8}$$

For more than 20 years, the investigation of decentralized hydrogen production with chemical looping systems is a particular part of the research work in the Working Group Fuel Cells and Hydrogen at Graz University of Technology. Hacker [10] proposed a fixed-bed chemical looping system for high-purity hydrogen production from renewable feedstock such as biogas, gasified biomass and more. The fixed-bed configuration is characterized by its simple and compact process design, which is especially beneficial for small-scale applications. It consists of a steam reformer and a fixed-bed chemical looping section within one tubular reactor, which enables concurrent hydrogen production and purification [10]. Thermodynamic simulations showed a process efficiency up to 84% considering optimized heat management [11].

In recent years, massive theoretical and experimental effort was spent to understand decisive effects of catalyst deactivation to improve the stability of applied catalysts. A comprehensive review of all relevant deactivation mechanisms was proposed by Argyle and Bartholomew [8]. Appari *et al* [12] developed a detailed kinetic model for steam reforming including hydrogen sulfide as representative trace gas. The results predict that the sulfur coverage is significantly high at the reactor inlet in the initial phase and moves downwards through the catalyst bed with time. Additionally, the results underline the strong temperature dependency of sulfur chemisorption on catalysts as high temperatures led to less sulfur coverage. Furthermore, Alstrup *et al* [13] obtained a relation to estimate equilibrium sulfur surface coverage for a $Ni/MgAl_2O_4$ catalyst in the temperature range of 773–1023 K and a H_2S concentration range from 7 to 50 ppm. The experimental data was validated well up to about 90% of saturation and was derived from the combination of Langmuir and Temkin isotherms. This approach was required since the mechanism of the adsorption violates the assumptions of the Langmuir isotherm. The study of Sadooghi and Rauch [14] presents a two dimensional pseudo-heterogeneous model to simulate SMR reactions in a packed bed tubular reactor considering various concentrations of sulfur in the feed gas. The influence of relevant process parameters such as H_2S concentration, S/C ratio, temperature and space velocity on the conversion of methane was investigated.

In context to chemical looping technologies, most literature about the impact of H_2S refers to CLC and CLOU [15–18]. However, hardly any literature can be found on the fate of sulfur in CLH processes. Within this work, an extensive experimental investigation of the selective deactivation of a commercial steam reformer catalyst with H_2S in pure methane and biogas reforming has been conducted in a small-scale fixed-bed reactor system. Kinetic modeling of the catalyst deactivation predicted the conversion of methane and synthetic biogas depending on various hydrogen sulfide concentrations. To gather additional profound information about the effect of sulfur coverage on the morphology of the catalyst, comprehensive techniques such as SEM/EDS and BET analysis were performed.

2. Experimental

2.1. Materials

The experimental investigation was carried out on a commercial steam reforming catalyst, comprised by nickel oxide (11.0 wt%) dispersed on an alumina oxide/calcium aluminate support ($CaAl_{12}O_{19}$). It was provided as pellets (3 mm) in oxidized state and thus required an initial reduction step prior to the reforming. To ensure a homogeneous gas and heat distribution in the reactor, the catalyst pellets were placed between fixed beds of 1 mm quartz glass beads (Sigmund Lindner).

2.2. Experimental setup

To investigate the deactivation of the reformer catalyst by sulfur, a test rig consisting of a gas supply unit, a fixed-bed reactor and a gas after treatment system was used (see figure 1). The catalyst pellets were placed in a quartz glass reactor ($d_i = 17$ mm, $L = 900$ mm) which was heated by an electrical tube furnace (Gero) to ensure the desired process temperature of 850 °C. The fixed-bed comprised by 30 g of catalyst was imbedded by quartz glass beads. In the center of the catalyst bed, a thermocouple was placed to monitor the bed temperature. As a safety measure, all inlets were equipped with normally closed solenoid valves (Burkert) which shut down in case of any malfunction. All gases were supplied by mass flow controllers (Bronkhorst, EL FLOW), controlled via LabView software. Water for the steam reforming was provided by a HPLC pump, vaporized by a coiled evaporator. To analyze the feed gases, a bypass line was installed upstream the reactor. All product gases leaving the reactor passed a heating line (Winkler WAKW) which avoided the condensation of steam and thus the dissolution of sulfur compounds. Furthermore, the off-gas entered PTFE condensers (wash bottles). They were filled with 1 M sulfuric acid, cooled down to 4 °C to condense steam in the product gas, but at the same time avoid the dissolution of H_2S. All gases were analyzed by a gas chromatograph (Inficon μGC Fusion).

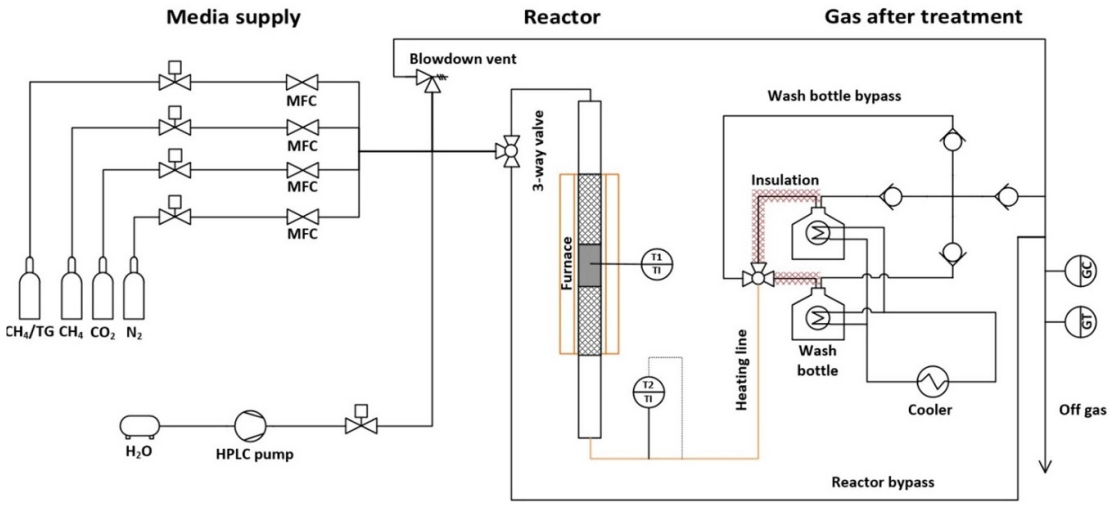

Figure 1. Schematic representation of the test rig.

Table 1. Overview of experiments with pure methane for various process conditions.

S/C (-)	Temperature (°C)	H_2S (ppm)
1.1	850	0
		5
		10
1.6	850	0
		0.5
		1
		5
		10
2	850	0
		0.5
		1
		5
		10
	750	0
		0.5
		1
		5
		10
	650	0
		0.5
		1
		5
3	850	0
		0.5
		1
		5
		10

2.3. Experimental procedure

Numerous experimental runs were performed with methane as well as synthetic biogas as feed gas. The first experimental campaign was performed with pure methane to gather fundamental information about the process behavior and the influence of temperature and S/C ratio (equation (9)) on the reforming efficiency. Afterwards, predefined concentrations of hydrogen sulfide were added to the feed gas to investigate the deactivation of the reformer catalyst (see table 1). The S/C ratio is defined as follows:

$$\mathrm{S/C} = \frac{\dot{n}^{\mathrm{in}}_{\mathrm{H_2O}}}{\dot{n}^{\mathrm{in}}_{\mathrm{CH_4}}} \overset{\mathrm{IG}}{=} \frac{\dot{V}^{\mathrm{in}}_{\mathrm{H_2O}}}{\dot{V}^{\mathrm{in}}_{\mathrm{CH_4}}}. \tag{9}$$

Table 2. Overview of experiments with synthetic biogas at 850 °C and various H_2S concentrations.

O/R (-)	H_2S (ppm)
2.8	0
	5
	10
3.8	0
	1
	5
	10
4.4	0
	1
	5

In the Biogas$_2$H$_2$ research project, the on-site production of high-purity hydrogen from raw biogas was demonstrated with a 10 kW_{th} RESC prototype system [19]. To predict the process behavior in utilizing raw biogas in the reformer section of the RESC, the composition of the local produced biogas was simulated within the reformer tests. Therefore, synthetic biogas comprised by 55 vol% of methane and 45 vol% of carbon dioxide contaminated with selective concentrations of H_2S was used as feed gas. An overview of the experiments with synthetic biogas at 850 °C is given in table 2.

Since biogas contains CO_2 as an oxidant, the introduction of the O/R ratio, the ratio between oxidative compounds and reductive compounds is introduced with (equation (10)):

$$\mathrm{O/R} = \frac{\dot{n}^{\mathrm{in}}_{\mathrm{H_2O}} + \dot{n}^{\mathrm{in}}_{\mathrm{CO_2}}}{\dot{n}^{\mathrm{in}}_{\mathrm{CH_4}}} \overset{\mathrm{IG}}{=} \frac{\dot{V}^{\mathrm{in}}_{\mathrm{H_2O}} + \dot{V}^{\mathrm{in}}_{\mathrm{CO_2}}}{\dot{V}^{\mathrm{in}}_{\mathrm{CH_4}}}. \tag{10}$$

The values for the O/R ratio were chosen in a way that the resulting S/C ratio values were equal to those used in the experiments with pure methane.

2.4. Physical characterization of catalyst

To gather more information on the effects of catalyst poisoning, fresh, poisoned and regenerated catalyst samples were analyzed by SEM/EDS and BET analysis. For the SEM and EDS analysis, a microscope equipped with a Zeiss Supra 35 VP (Carl Zeiss, Oberkochen, Germany) including an EDS spectrometer silicon drift detector EDS Ultim Max 100 (Oxford Instruments, Oxford, UK) was applied. The operative voltage was set to 5 kV for SEM and 20 kV for EDS. For the BET analysis, a fully automated Tristar II system (Micromerits) was used. Nitrogen 5.0 served as adsorptive gas. The detection limit of the regarding system was 0.01 $m^2\ g^{-1}$.

2.5. Key performance indicators

To describe the impact of H_2S on the reaction behavior and performance of the applied catalyst, various key performance indicators were defined (see table 3). The chemisorption of H_2S leads to the blocking of active sites of the catalyst otherwise available for the preferred reaction. The progress of deactivation can be quantitatively characterized by the decrease in methane conversion (equation (11)) during reforming. Furthermore, the influence of sulfur chemisorption on the water gas shift reaction can be evaluated according to (equation (12)). The selectivities of H_2 related to CO and CO_2 are defined in line with the work of Fogler [20].

The carbon mass balances around the steam reforming unit were established as a means of increasing the significance of the experiments. At first, the total gas flow was calculated from the amount of standard gas V_{N2} and the volume fraction of nitrogen y_{N2} (equation (19), table 4). Based on the total gas flow, the volume flows of all other gases were determined according to (equations (20)–(22)). The quantities of carbonaceous gases leaving and entering the system are calculated according to (equations (23)–(25)). The mass balance error is given by (equation (26)). The error was calculated for all μGC measurement points (i) throughout the reduction phase.

In figure 2, a trend of the carbon mass balance error for a representative reforming test is given. Apart from unstable process behavior at the beginning of the experiment, a uniform trend for more than 11 h of operation can be seen. The mean mass balance error varied between 4% and 6%. It can be explained by several potential error sources such as the calibration of the μGC with 2%. In addition, the calibration of the used mass flow controller can cause inaccuracies of 2–3%.

Table 3. Key performance indicators.

Indicators	Equation	Unit	Equations
Methane conversion	$X_{CH_4} = \frac{\dot{n}^{react}_{CH_4}}{\dot{n}^{in}_{CH_4}} = \frac{\dot{n}^{in}_{CH_4} - \dot{n}^{out}_{CH_4}}{\dot{n}^{in}_{CH_4}}$	(-)	(11)
Carbon monoxide conversion	$X_{CO} = \frac{\dot{n}^{react}_{CO,WGS}}{\dot{n}^{in}_{CO}} = \frac{\dot{n}^{out}_{CO_2}}{\dot{n}^{out}_{CO} + \dot{n}^{out}_{CO_2}}$ or $\frac{\dot{n}^{out}_{CO_2}}{X_{CH_4}\dot{n}^{in}_{CH_4}}$	(-)	(12)
Selectivity of H_2 vs CO	$S_{H_2,CO} = \frac{\dot{n}^{out}_{H_2}}{\dot{n}^{out}_{CO}}$	(-)	(13)
Selectivity of H_2 vs CO_2	$S_{H_2,CO_2} = \frac{\dot{n}^{out}_{H_2}}{\dot{n}^{out}_{CO_2}}$	(-)	(14)
Selectivity of H_2 vs CO and CO_2	$S_{H_2,CO+CO_2} = \frac{\dot{n}^{out}_{H_2}}{\dot{n}^{out}_{CO} + \dot{n}^{out}_{CO_2}}$	(-)	(15)
Carbon accumulation	$m^{acc}_{C,k} = m^{acc}_{C,k-1} + \left(\dot{m}^{in}_{C,k} - \dot{m}^{out}_{C,k}\right)(t_k - t_{k-1})$	(g)	(16)
Sulfur accumulation	$m^{acc}_{S,k} = m^{acc}_{S,k-1} + \left(\dot{m}^{in}_{S,k} - \dot{m}^{out}_{S,k}\right)(t_k - t_{k-1})$	(g)	(17)
Activity	$a = \frac{X_{CH_4}(t_k)}{X_{CH_4}(t_k=0)}$	(-)	(18)

Table 4. Calculation of mass balance error.

Description	Equation	Unit	Equation
Total volume flow	$V_{tot} = \frac{V_{N_2}}{y_{N_2}}$	(Nl min^{-1})	(19)
Volume flow CH_4	$V_{CH_4} = V_{tot} * y_{CH_4}$	(Nl min^{-1})	(20)
Volume flow CO_2	$V_{CO_2} = V_{tot} * y_{CO_2}$	(Nl min^{-1})	(21)
Volume flow CO	$V_{CO} = V_{tot} * y_{CO}$	(Nl min^{-1})	(22)
Molar flow CH_4	$\dot{n}_{CH_4,i} = \frac{\dot{V}_{CH_4}}{v_m}$	(mol min^{-1})	(23)
Molar flow CO_2	$\dot{n}_{CO_2,i} = \frac{\dot{V}_{CO_2}}{v_m}$	(mol min^{-1})	(24)
Molar flow CO	$\dot{n}_{CO_2,i} = \frac{\dot{V}_{CO}}{v_m}$	(mol min^{-1})	(25)
Carbon mass balance relative error	$E_{CMB,i} = 1 - \frac{\left(\dot{n}^{out}_{CH_4} + \dot{n}^{out}_{CO_2} + \dot{n}^{out}_{CO}\right)MM_C}{\dot{n}^{in}_{CH_4} MM_C}$	(-)	(26)

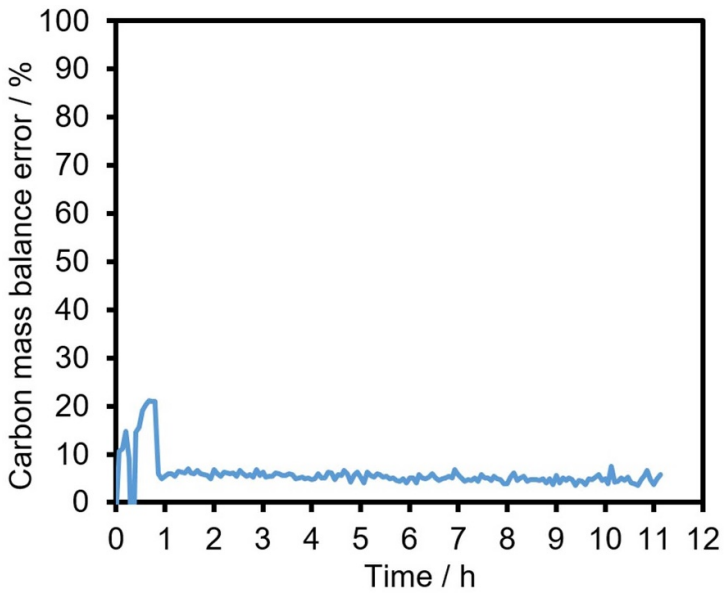

Figure 2. Course of carbon mass balance error.

Table 5. Stoichiometric matrix of considered reactions.

Reaction	CH_4	H_2O	H_2	CO	CO_2
R1 (SMR)	−1	−1	3	1	0
R2 (WGS)	0	−1	1	−1	1
R3 (RM)	−1	−2	4	0	1

3. Kinetic modeling of catalyst deactivation

The packed bed reactor has been modeled as a one-dimensional pseudo-homogeneous non-isothermal plug flow reactor. The assumptions of the developed model are similar to those made by Halabi *et al* [21]:

(a) Ideal gas conditions, since the process takes place at high temperature and atmospheric pressure.
(b) Radial gradients of concentration and temperature are negligible.
(c) Catalyst particles are uniform in shape and size.
(d) The internal mass transfer resistance in the catalyst pellet is negligible since pores are absent.
(e) The void fraction of the packed bed is constant, both axially and radially.
(f) Pressure drops are negligible due to the small bed length ($h \sim 13$ cm). The reactor can be considered isobaric, thus the momentum balance has been neglected.
(g) The reactor is uniformly heated along its length, the power of the furnace is proportional to the difference between the constant temperature of the furnace and the temperature of the reactor.
(h) The reaction kinetic proposed by Xu and Froment [22] is assumed. It postulates the presence of five species: CH_4, H_2O, H_2, CO and CO_2, and three reactions (SMR, WGS and RM). The model was developed for a $Ni/MgAl_2O_4$ catalyst with a nickel surface area of 3 $m^2\ g^{-1}$. The catalyst in the regarding investigation had a nickel surface area of 1.1 $m^2\ g^{-1}$. For biogas reforming the dry reforming reaction scheme is neglected.
(i) Carbon formation reactions are also neglected, since it is prevented by S/C ratios above 2.
(j) Reformer operation is considered under steady state flow conditions.

3.1. Conservation equations

Based on the above assumptions, the mass and energy balances have been formulated considering an infinitesimal mass of catalyst (dm_{cat}).

The mass balance for a generic species *i* is given by:

$$\frac{d\dot{n}_i}{dm_{cat}} = \sum_j^{NR} \nu_{j,i} R_j'^{,S} \eta_j. \tag{27}$$

The five mass balances can be written as the scalar product of the stoichiometric matrix and the reaction rate vector. The stoichiometric matrix ($\nu_{j,i}$) is reported in table 5.

The energy balance of the non-isothermal reactor is given by:

$$\frac{dT}{dm_{cat}} = \frac{\hat{A}h\,(T_f - T) + \sum_j^{NR}\left(-\Delta\tilde{H}^{\circ}_{R,j}\right) R_j'^{,S}\eta_j}{\sum_i^{NC} \dot{n}_i \tilde{c}_{p,i}} \tag{28}$$

The product $\hat{A}h$ of the specific pellet surface area and the pellet heat transfer coefficient (equation (30)) was computed using the Newton's law of cooling:

$$\dot{Q} = Ah\,(T_f - T)\,. \tag{29}$$

It was expressed with respect to a unit mass of catalyst. Using the furnace maximum heat transfer rate of $\dot{Q}_{max} = 2.8\,kW$ for $\Delta T_{max} = 1200\ °C$, a simple calculation yields the following result:

$$\hat{A}h = \frac{1}{m_{cat}} Ah = \frac{1}{m_{cat}} \frac{\dot{Q}}{\Delta T_{max}} = 0.28\,kJ\,(h\,g\,K)^{-1}. \tag{30}$$

Table 6. Reaction rates for steam methane reforming by Xu and Froment [22].

Reaction	Rate equation	
SMR	$R_1' = R_{1,\text{for}}' - R_{1,\text{back}}' = \frac{\frac{k_1}{p_{H_2}^{2.5}}\left(p_{CH_4}p_{H_2O} - \frac{p_{H_2}^3 p_{CO}}{K_{p1}}\right)}{DEN^2}$	(31)
WGS	$R_2' = R_{2,\text{for}}' - R_{2,\text{back}}' = \frac{\frac{k_2}{p_{H_2}}\left(p_{CO}p_{H_2O} - \frac{p_{H_2}p_{CO_2}}{K_{p2}}\right)}{DEN^2}$	(32)
RM	$R_3' = R_{3,\text{for}}' - R_{3,\text{back}}' = \frac{\frac{k_1}{p_{H_2}^{3.5}}\left(p_{CH_4}p_{H_2O}^2 - \frac{p_{H_2}^4 p_{CO_2}}{K_{p3}}\right)}{DEN^2}$	(33)

Table 7. Parameters of reaction rate, equilibrium, and adsorption of the kinetic model for steam methane reforming [22].

Constant	Equation	Parameters	
Reacting rate	$k_j = A_j e^{-\frac{E_{a,j}}{RT}}$	$A_1 = 4.225 \cdot 10^{15}$	$E_1 = 240.1$
		$A_2 = 1.955 \cdot 10^{6}$	$E_2 = 67.13$
		$A_3 = 1.020 \cdot 10^{15}$	$E_3 = 243.9$
Equilibrium	$K_{pj} = e^{\frac{\Delta s_{Rj}^0}{R} + \frac{\Delta H_{Rj}^0}{T}} = e^{a_j + \frac{b_j}{T}}$	$a_1 = 30.481$	$b_1 = -27.187$
		$a_2 = -3.924$	$b_2 = 4.291$
		$a_3 = 26.891$	$b_3 = -23.258$
Adsorption	$K_i = A_i e^{-\frac{\Delta H_i}{RT}}$	$A_{CH_4} = 6.65 \cdot 10^{-4}$	$\Delta\tilde{H}_{CH_4} = -38.28$
		$A_{H_2O} = 1.77 \cdot 10^{5}$	$\Delta\tilde{H}_{H_2O} = 88.68$
		$A_{H_2} = 6.12 \cdot 10^{-9}$	$\Delta\tilde{H}_{H_2} = -82.90$
		$A_{CO} = 8.23 \cdot 10^{-5}$	$\Delta\tilde{H}_{CO} = -70.65$

3.2. Reaction rates

The kinetic model proposed by Xu and Froment [22] has been adopted. The three reaction rates expressed considering a unit mass of catalyst, are summarized in table 6.

The denominator of the reaction rates is given by (equation (34)):

$$DEN = 1 + K_{CO}p_{CO} + K_{H_2}p_{H_2} + K_{CH_4}p_{CH_4} + K_{H_2O}\frac{p_{H_2O}}{p_{H_2}}. \tag{34}$$

The reaction rate parameters are:

- $k_{1,2,3}$, reaction rate constants with kmol bar$^{0.5}$ kg^{-1} h^{-1} for reactions SMR and RM and kmol bar^{-1} kg^{-1} h^{-1} for the WGS reaction.
- $K_{p1,p2,p3}$, equilibrium constants based on partial pressure. The unit of measurements are bar^2 for reactions SMR and RM and none for reaction WGS.
- K_{CO,H_2,CH_4,H_2O}, adsorption equilibrium constants. The unit of measurements are bar^{-1} for all species except for the constant regarding water, which is dimensionless.

These parameters are functions of temperature according to the equations reported in table 7. The unit of measurement for $E_{a,j}$ and $\Delta\tilde{H}_i$ is kJ mol^{-1}, whereas those of the pre-exponential factors are equal to those of the constants that they define.

As suggested by Cipitì *et al* [23] and by Halabi *et al* [21], each reaction rate is weighted by an effectiveness factor (η_j) to consider the intra-particle transport limitation. In the regarding model, a single value was applied to the three reaction rates, i.e. $\eta = \eta_j = 0.001$ for $j = 1, 2, 3$. However, the determination of specific effectiveness factors for all three reforming reactions could further increase the accuracy of the prediction.

3.3. Sulfur coverage

Rostrup-Nielsen [24] used a Maxted model to express the (surface specific) poisoned reforming rate of a nickel catalyst ($R''^{,S}$) as a function of the (surface specific) unpoisoned reforming rate (R'') and the fraction of sulfur-free catalyst sites ($1 - \theta_S$). The rates are expressed per unit of Ni active area and so the unit of measurement is mol m^{-2} h^{-1}, whereas the coverage is dimensionless (see equation (35)). Obviously, at full coverage ($\theta_S = 1$) the catalyst is completely deactivated, and the reforming rate equals zero:

$$R''^{,S} = R''(1 - \theta_S)^3. \tag{35}$$

Thanks to the latter, equations (31)–(33) can be used to compute the poisoned reaction rates. However, since the unpoisoned rate (equation (35)) is expressed per unit of free Ni surface, it is necessary to multiply it

Table 8. Parameters for calculation of molar heat capacities.

Parameter	CH_4	H_2O	H_2	CO	CO_2
$a_i \cdot 10^3$	5.529	1.558	0.370	0.716	1.593
b_i	3.292	3.409	3.266	3.269	4.925

by the Ni surface area of the used catalyst. Thus, the unit of the rates changes from mol $m^{-2}{}_{N2}$ h^{-1} to mol $g^{-1}{}_{cat}$ h^{-1} and (equation (35)) is adapted to equation (equation (36)):

$$R_j'^{,S} = \hat{S} \cdot R_j'' (1-\theta_S)^n = R_j' (1-\theta_S)^3. \tag{36}$$

This relationship allows estimating the outlet molar flow rates as a function of the sulfur coverage instead of a function of time, what simplifies the work.

3.4. Molar enthalpies and heat capacities

The molar enthalpies of reactions (kJ mol^{-1}) have been computed using (equations (37)–(39)) based on [22]:

$$\Delta\tilde{H}_{R,1}(T) = 226.9 - 4.47 \cdot 10^{13} T^{-4.459} \tag{37}$$

$$\Delta\tilde{H}_{R,2}(T) = -271.4 T^{-0.2977} \tag{38}$$

$$\Delta\tilde{H}_{R,3}(T) = 99.52 T^{0.0937} \quad . \tag{39}$$

The ideal gas molar heat capacities (kJ mol^{-1} K^{-1}) of each species have been approximated by equation (40). Its coefficients are reported in table 8:

$$\tilde{c}_{p,i}(T) = R(a_i T + b_i). \tag{40}$$

3.5. System of equations

The ODE system, composed of five mass balances and one energy balance, has been numerically solved using the ODE15s solver of MATLAB 2020b.

Considering the mass of catalyst used in the experiments ($m_{cat} = 30$ g) and a value of the coverage ($\theta s = 0$ for sulfur-free experiments), the simulation yields the reactor outlet molar flow rates of each species and the outlet temperature. Moreover, by solving the system for different values of θs, one can compute the profile of the molar flow rates during the poisoning. These profiles are a function of the sulfur coverage and independent of time. The experimental coverage was expressed as a function of the residual activity only:

$$\theta_{S,exp} = 1 - a_{exp} = 1 - \frac{X_{CH_4,exp}(t)}{X_{CH_4,exp}(0)}. \tag{41}$$

The validity of this model was assessed by comparing the predicted results with the experimental data. In general, the model can be used to estimate either the value of the coverage by knowing the conversion or the residual conversion. The latter can be either experimentally measured, as done in this work, or computed by (equation (42)) according to Alstrup *et al* [13]. If applied in a steady state process, one has to assume a constant inlet sulfur flow rate:

$$\theta_S = 1.45 - 9.53 \cdot 10^{-5} T + 4.17 \cdot 10^{-5} T \ln\left(\frac{p_{H_2S}}{p_{H_2}}\right). \tag{42}$$

4. Results and discussion

4.1. Catalyst deactivation in methane reforming

The dry equilibrium composition of the reacting gases was determined by a preliminary thermodynamic study. Calculations were performed using the program Chemical Equilibrium with Applications, NASA, which calculates chemical equilibrium compositions as well as thermodynamic and transport properties of complex mixtures. One mole of methane has been assumed as the basis for the calculations.

The results for $T_{op} = 850$ °C and various steam to carbon ratios are reported in figure 3. In general, the predicted equilibrium mole fractions are in good accordance to the experimental data. The deviation of the hydrogen composition is smaller than 2%, further a slightly higher deviation of 1%–4% for methane was

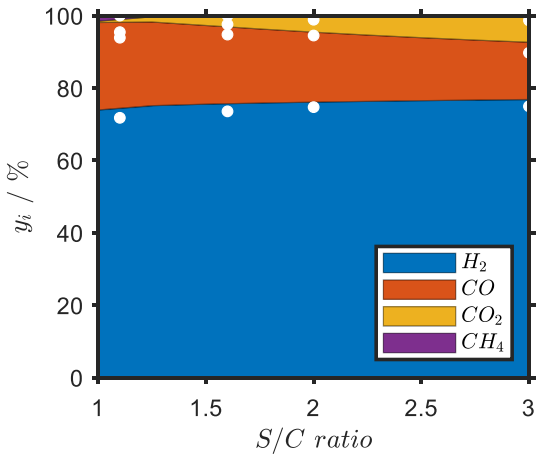

Figure 3. Molar composition of product gas at chemical equilibrium for $T_{op} = 850\,°C$ with simulated data in colors (H_2 in blue, CO in orange, CO_2 in yellow and CH_4 in purple) and experimental data represented by white dots.

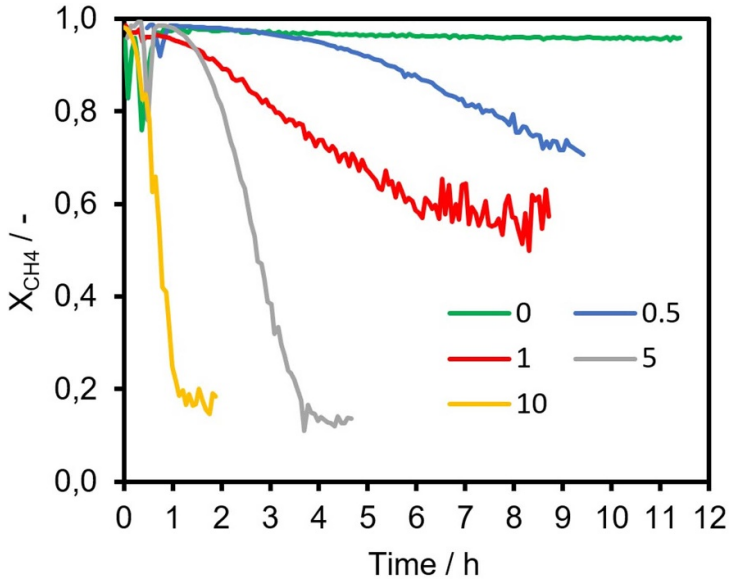

Figure 4. Deactivation curves for steam methane reforming for different H_2S concentrations in ppm.

determined. As expected, the CO_2 molar fraction increases as the S/C ratio increases, since the excess of water favors the WGS reaction. However, this effect is thermodynamically hindered by the high operating temperature.

To quantify the negative impact of H_2S on the activity of the reformer catalyst, defined concentrations of H_2S were added to the methane feed gas. The conversion of methane during the deactivation cycle is plotted versus time for H_2S concentrations of 0.0, 0.5, 1.0, 5.0 and 10 ppm as shown in figure 4. The deactivation rate and the extend of deactivation directly correlate with the hydrogen sulfide concentration. The same deactivation behavior was observed by Appari *et al* [12, 25], or Chiodo *et al* [6] in previous studies. For concentrations of 0.5 and 1.0 ppm H_2S, the deactivation rate (slope of curve) is similar, whereas the final residual methane conversion in the considered process time is only comparable for H_2S concentrations of 5 ppm and 10 ppm. The final conversion rate for $[H_2S] = 5$ ppm and $[H_2S] = 10$ ppm is comparable (17% and 20%), though it was reached after 1.5 h and 4.0 h. Summarizing, the deactivation rate increases and the final residual methane conversion is lower and faster reached with an increasing hydrogen sulfide concentration.

To validate the experimental data for catalyst deactivation in SMR, a model for a one-dimensional pseudo-homogeneous non-isothermal plug flow reactor was developed. In general, the simulated data is in good accordance to the experimental results in terms of methane conversion as a function of sulfur coverage (see figure 5). The experimental conversions are straight lines when plotted against the sulfur coverage. This

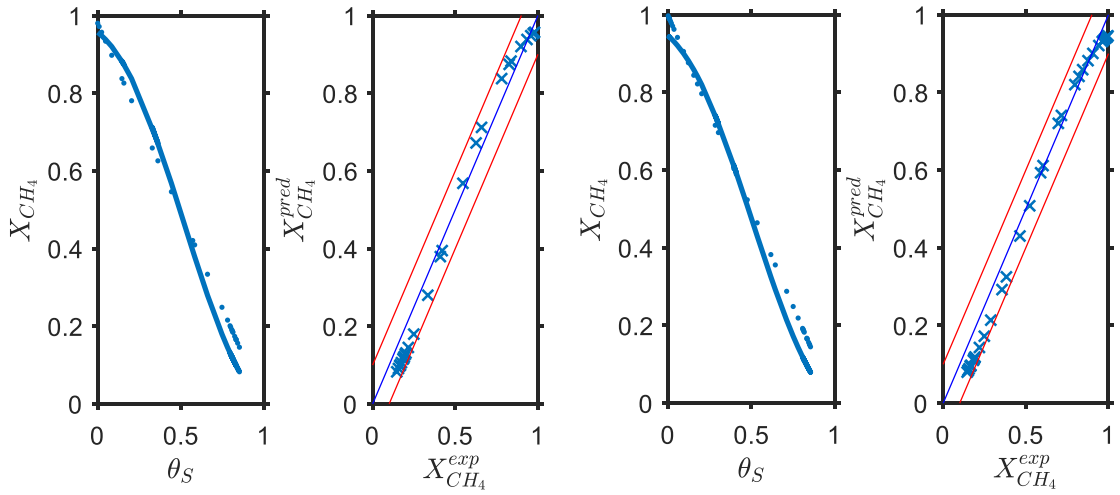

Figure 5. Predicted (full lines) versus experimental (dots) methane conversion and parity plots for the steam methane reforming experiments at S/C 2 (left) and S/C 3 (right), $T = 850$ °C and $[H_2S] = 10$ ppm.

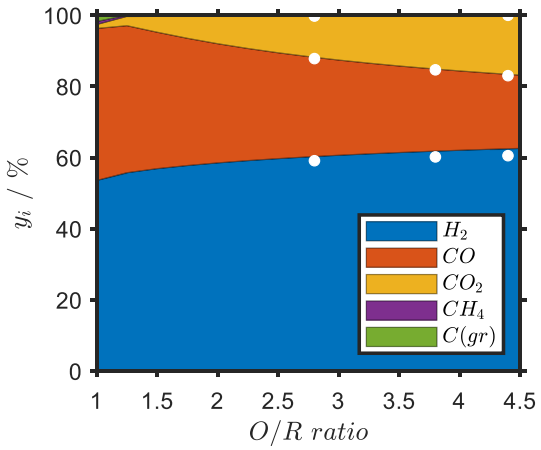

Figure 6. Molar composition of product gas at chemical equilibrium for $T_{op} = 850$ °C with simulated data in colors (H_2 in blue, CO in orange, CO_2 in yellow, CH_4 in purple and carbon in green) and experimental data in white dots.

is caused by the definition of the sulfur coverage (see equation (41)). One can note that the model slightly overestimates the methane conversion for $\theta < 0.4$ and gives lower values for $\theta > 0.6$. This is caused by the constant effectiveness factor of 0.001 for all reactions. More accurate results can be expected if a specific effectiveness factor would be determined for each of the three reactions. In this case, the intra-particle transportation limit would be considered in more detail.

The red lines of the parity plots represent the ±10% deviations from the experimental value. The predicted results lie within this band and hence the deviation between experimental and simulated data is <10%. The applied model works well for high temperatures of >800 °C, whereas for lower temperatures the effectiveness factor needs to be adjusted to restore a feasible prediction of the experimental results.

4.2. Catalyst deactivation in biogas reforming

As for SMR, a preliminary study on the chemical equilibrium dry composition was also performed for biogas reforming. The results are reported in figure 6, the white dots represent the average experimental composition without steam and nitrogen.

For pure biogas, the experimental compositions are 1% and 2% below or above the equilibrium ones, confirming that the reactions for this operating temperature can be considered at the equilibrium. The results are in better accordance compared to those of SMR. Furthermore, the carbon dioxide molar fraction increases with increasing oxidant to reductant ratio, since the excess of water favors the water gas shift reaction. Thus, the fraction of hydrogen is below 65%, while for pure methane (see figure 3) the lowest volume fraction was 75%.

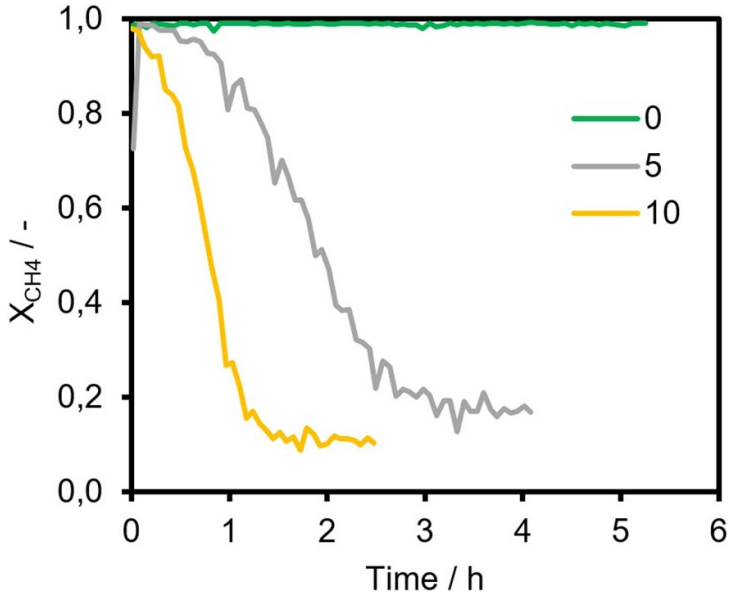

Figure 7. Deactivation curves in biogas reforming for O/R = 2.8 and different H_2S concentrations in ppm at $T = 850$ °C.

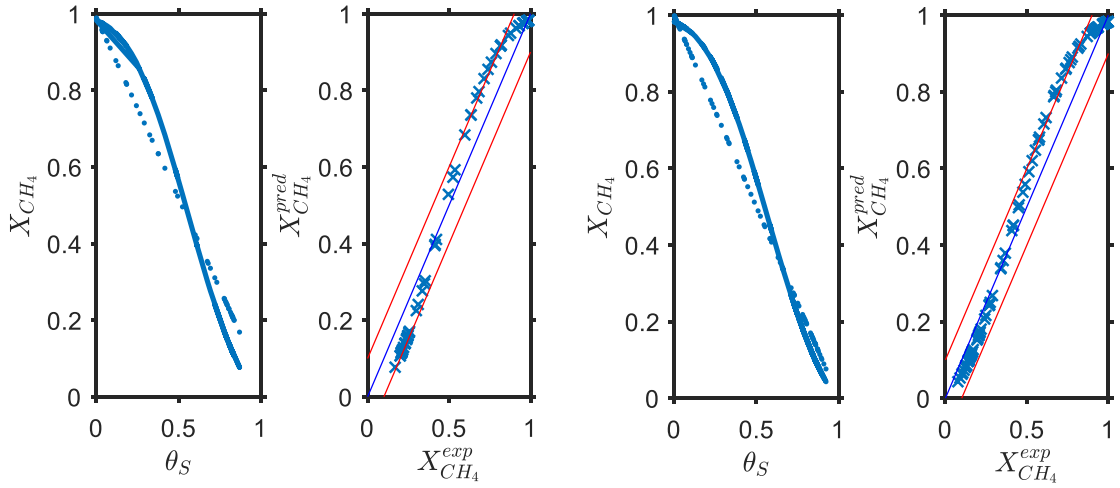

Figure 8. Predicted (full lines) versus experimental (dots) methane conversion data and parity plots for biogas reforming experiments at O/R 2.8 (left) and O/R 3.8 (right), $T = 850$ °C and $[H_2S] = 10$ ppm.

Figure 7 shows the impact of different hydrogen sulfide concentrations (0.0, 5.0 and 10 ppm) on the methane conversion in biogas reforming. The behavior is analogous to methane reforming as the deactivation rate increases with increasing H_2S concentration. The residual methane conversion for $[H_2S] = 10$ ppm is even 10% lower compared to the SMR experiments after the same process time. This hypothesis also correlates with the temperature course in the reactor bed. For the SMR process, a bed temperature of 831 °C was measured at the final conversion. In the biogas experiment, a reactor temperature of 839 °C was measured, what underlines the lower endothermicity caused by the hindered reforming reaction. Thus, the impact of hydrogen sulfide on biogas reforming seems stronger compared to pure methane reforming.

The experimental and predicted conversion profiles for two O/R ratios, $T_{op} = 850$ °C and $[H_2S] = 5$ ppm are given in figure 8. One can note that at high sulfur coverages the quality of the prediction increases with the O/R ratio. In any case, all predicted conversions are bounded between the 10% errors, except for some values of θ_S between 0.6 and 0.8. For the biogas feedstock, the conversion values are also overestimated for high coverages and underestimated for low, whereas the relative error is close to zero for intermediate coverages. Similar accuracies have been obtained for the data at the same operating point with $[H_2S] = 10$ ppm, which are not reported here.

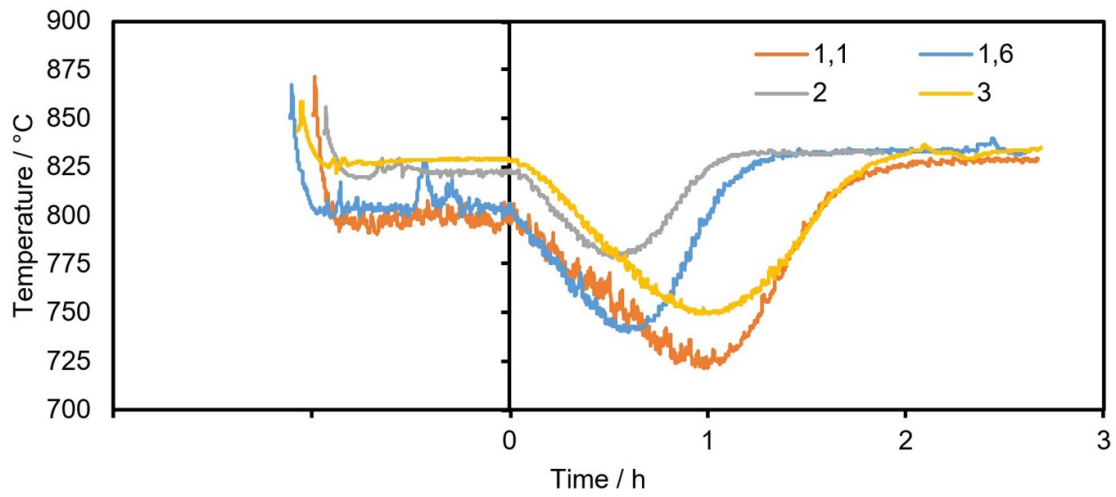

Figure 9. Catalyst bed temperature for steam methane reforming with various S/C ratios, $T = 850\ ^{\circ}C$ and $[H_2S] = 5$ ppm.

To overcome the described catalyst deactivation effects, the application of highly-stable Ni catalysts supported by Mg or $LaAlO_3$ is suggested in literature [26, 27]. To evaluate the sulfur resistance of those catalysts in real gas reforming conditions would be a possible next step in this research field.

4.3. Temperature effect

When poisonous hydrogen sulfide is added to the feed gas, the (endothermic) steam reforming reaction is strongly hindered, so one would expect that the reactor temperature increase. However, the temperature measurement of the catalyst bed showed different results as one can see in figure 9. In this chart, the time scale starts at $t = 0$ when H_2S was fed into the system. In the time range before $t = 0$, conventional reforming took place. The temperature started to decrease at $t = 0$, what was not expected prior to the experiments.

In general, one has to consider that:

(a) There is a single thermocouple located in the center of the reactor.
(b) Only few ppm of H_2S are introduced.
(c) According to Rostrup-Nielsen and Christiansen [28], sulfur chemisorbs on the first pellets it encounters, those on the top of the reactor. When their active sites are saturated, the sulfur reaches the next pellets.
(d) The reaction front (zone in which the reaction rates are at their maximum) is present at the top of the bed and moves downwards.

Accordingly, it was concluded that the catalyst deactivation moves the reforming reaction front towards the bottom of the reactor. Therefore, the reactor temperature initially decreases as the reaction front approaches the thermocouple, reaches a minimum when the front is in the center of the catalytic bed and increases again as the front moves towards the bottom of the reactor.

It can be noted that the minimum reaction temperature is reached at half of the time needed to achieve the final temperature. Additionally, the reactor temperature profile has a reverse bell-like shape. Considering that the thermocouple is located in the center of the catalytic bed, one can assume that the reaction front moves with constant speed towards the bottom of the bed.

4.4. Catalyst regeneration

The chemisorption of sulfur on the active sites of catalysts is a reversible reaction what allows the elimination of the adsorbed sulfur layer through regeneration methods. According to the works of Appari *et al* [25], Ashrafi *et al* [29] and Yang [30], four different regeneration techniques are suggested:

- Steam reforming without sulfur (removing H_2S from feed gas)
- Temperature increase
- Steam oxidation
- Air oxidation.

Hydrogen sulfide removal is proved as a sufficient regeneration method but the complete recover to reach the initial reforming rate is not possible. The rate and extend of the regeneration are influenced by the H_2S

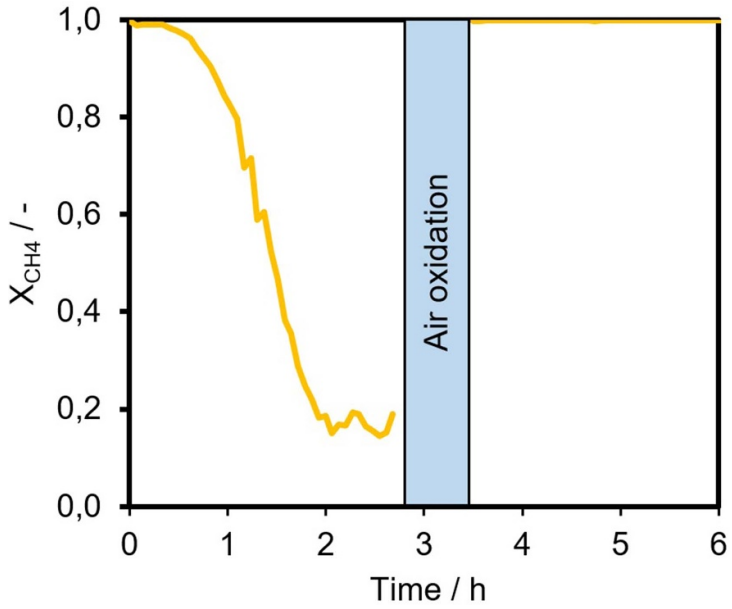

Figure 10. Catalyst deactivation and regeneration through oxidation with air.

Table 9. Overview of analyzed catalyst samples.

Sample	Performed experiment	State
0		Fresh
1	$T_{op} = 750\ ^{\circ}C$, S/C = 2, $[H_2S] = 1$ ppm	Deactivated by carbon
2	Regeneration	Regenerated
3	$T_{op} = 850\ ^{\circ}C$, S/C = 2, $[H_2S] = 10$ ppm	Deactivated by sulfur

Figure 11. Visual comparison of fresh (0, left), carbon deactivated (1, middle) and sulfur deactivated (2, right) catalyst samples.

feed gas concentration and the process temperature. In general, a hydrogen sulfide concentration of >50 ppm at a process temperature of <900 °C prevents a complete catalyst regeneration [30]. Since the temperature dependency of hydrogen sulfide chemisorption [8, 31] is pronounced, a process temperature enhancement is proposed to be a very effective regeneration technique. In combination with the first given method, the restoration of the original activity is possible even for high sulfur uptakes. Apart from that, the oxidation with steam and air allows the complete regeneration of deactivated steam reformer catalysts. Within this work, the oxidation with air and the regeneration through steam reforming without sulfur was performed.

A representative profile for the deactivation and regeneration of the regarding SMR catalyst using air as an oxidant is given in figure 10. After the deactivation with 10 ppm H_2S in the feed gas, a mixture of 50 vol% synthetic air and 50 vol% nitrogen with a flow rate of 1 Nl min^{-1} was fed to the reactor system for 15 min. It can be seen that the methane conversion was completely restored from approximately 20% at the end of the deactivation process.

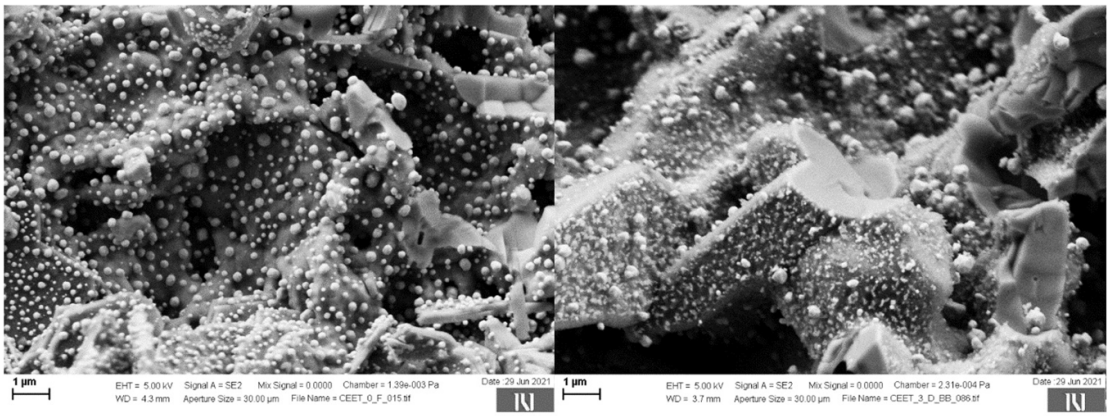

Figure 12. Morphology of fresh (left) and sulfur deactivated (right) catalyst with a magnification of 1 μm.

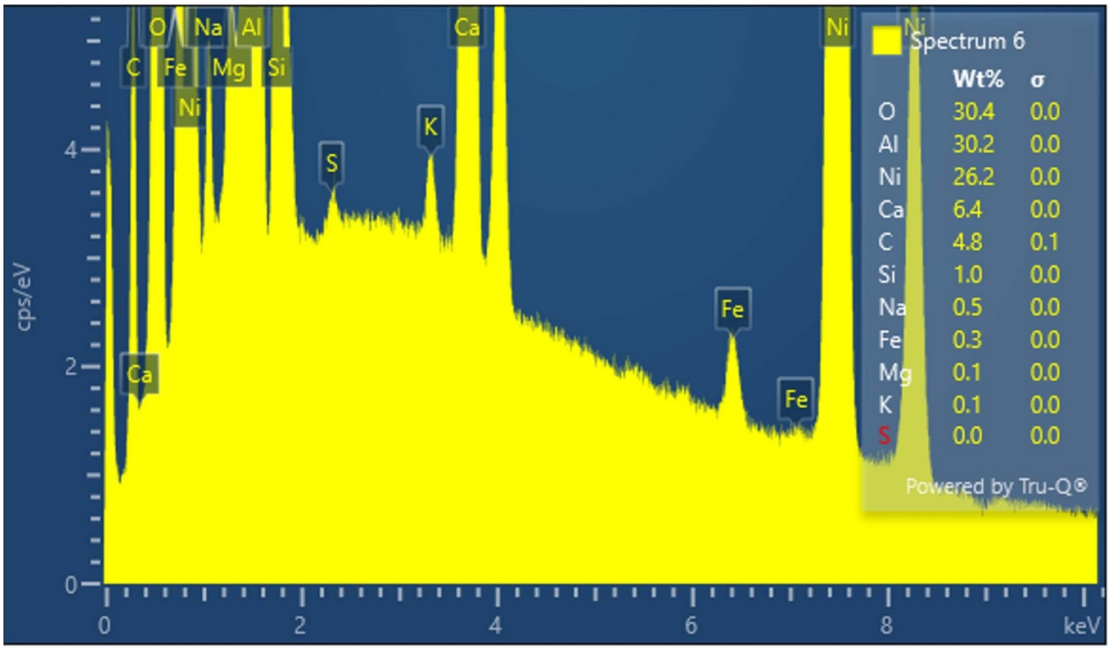

Figure 13. EDS pattern of a representative deactivated catalyst sample.

4.5. Physical characterization

To gather more information about the effects of catalyst poisoning on the morphology of the steam reformer catalyst, a comprehensive characterization of fresh, deactivated and regenerated catalyst samples applying SEM/EDS and BET techniques was made. Table 9 shows an overview of the analyzed samples. A visual comparison of three different catalyst samples is given in figure 11. The fresh catalyst (left) allows for a comparison. Sample 1 was deactivated through massive carbon deposition and is thus covered by a black powdery layer. The EDS analysis confirmed coal on the surface of the sample. Sample 2 was deactivated with H_2S and shows yellowish pellets. The color indicates the chemisorption of sulfur on the surface of the pellets.

In figure 12, a comparison of the morphology between fresh catalyst (left) and sulfur deactivated catalyst (right) is shown in SEM images. The fresh sample shows homogeneously distributed and well defined nickel particles on the clean surface of the carrier material. They have a narrow particle size distribution with a diameter of approximately 200–300 nm. In the right image, one can see that the surface of carrier material is covered by a sort of dust, which has an intermediate color between the dark grey of the support and the light grey of the active sites. This would suggest the presence of sulfur, both because its molar mass is in between the one of the support and nickel, and because the yellow color was perfectly visible to the bare eye.

To prove the presence of sulfur on the surface of the deactivated catalyst, EDS analysis was performed. The EDS pattern (figure 13) clearly shows the sulfur peak at 2.4 keV. However, the portion of sulfur equals

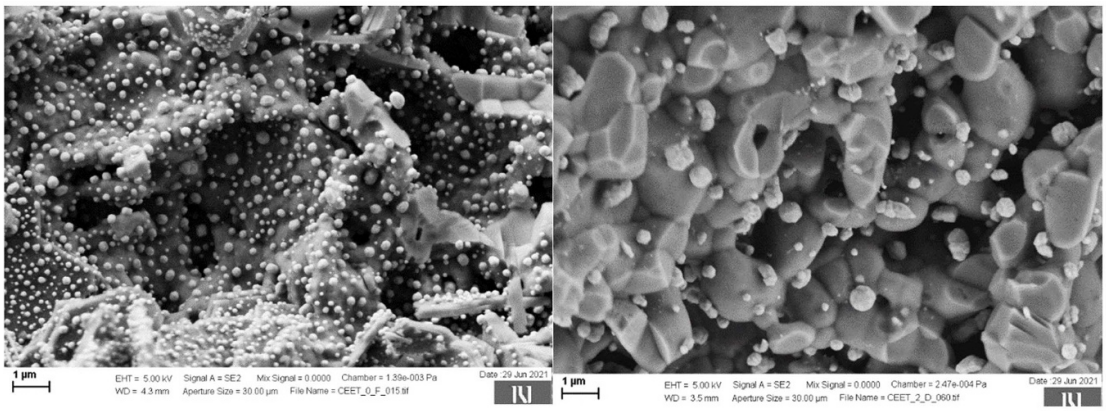

Figure 14. Morphology of fresh (left) and regenerated catalyst (right).

0.04 wt% and is thus nearly at the detection limit of the applied analysis system. In terms of the BET surface area, no significant difference between the fresh (1.0945 $m^2\ g^{-1}$) and the deactivated catalyst (1.1917 $m^2\ g^{-1}$) was observed. The slight increase (8%) of surface area due to sulfur adsorption fits to the fine dispersed morphology shown in figure 12 (right).

To evaluate the effectiveness of the regeneration, the morphology of the catalysts surface was characterized in addition to the determination of the biogas conversion. In figure 14, a comparison of fresh (left) and regenerated (right) catalyst is given. From a qualitative point of view, one can note that the nickel particles are still uniformly dispersed on the regenerated catalyst but the number and size of them changed. Indeed, it seems that less and larger particles are present. This evidence could suggest that due to the high temperatures of up to 1000 °C, sintering took place throughout the regeneration step. Nevertheless, the BET surface area of 1.1074 $m^2\ g^{-1}$ is the same compared to the fresh catalyst.

5. Conclusion

To determine the deactivation of a steam reformer catalyst for chemical looping hydrogen production, extensive experimental tests were conducted for reforming methane and synthetic biogas with impurities of 1, 5 and 10 ppm H_2S in the feed gas. Thermodynamic calculations were used to determine the equilibrium dry outlet composition with a deviation of 4% for SMR and 2% for synthetic biogas reforming compared to the experimental results.

The simulation of a one-dimensional pseudo-homogeneous plug flow reactor using a fitted Maxted model has successfully validated the experimentally determined deactivation behavior. The methane conversion as a function of sulfur coverage lies within a deviation of $<10\%$ for methane reforming and biogas reforming compared to the experimental results. Monitoring of the reactor bed temperature enabled the visualization of the reforming reaction front depending on the catalyst deactivation towards the bottom of the fixed-bed reactor. Air oxidation steps were performed to completely restore the initial reactivity of the reformer catalyst. A correct quantification was confirmed by the fulfillment of the carbon mass balance within a mean deviation of 5%. In addition, the impact of sulfur chemisorption on the morphology of the used reformer catalyst was investigated by SEM/EDS and BET techniques. In SEM patterns, the presence of sulfur in form of dust on the surface of the catalyst was ascertained. This hypothesis was confirmed by EDS analysis with a sulfur concentration of 0.04 wt%.

Data availability statement

The data that support the findings of this study are available upon reasonable request from the authors.

Acknowledgments

Financial support from the Austrian Research Promotion Agency (FFG) through the 30th Bridge Call supported by the Federal Ministry for Climate Action, Environment, Energy, Mobility, Innovation, and Technology (BMK), and also from the Federal Ministry for Digital and Economic Affairs (BMDW) is gratefully acknowledged. Supported by TU Graz Open Access Publishing Fund.

CrediT authorship contribution statement

Bernd Stoppacher: Conceptualization, methodology, investigation, writing-original draft.
Francesco Lonardi: Methodology, investigation, development of kinetic model, writing-original draft.
Sebastian Bock: Conceptualization, writing-review & editing.
Marjan Bele: Characterization of catalyst samples with (SEM/EDS).
Alberto Bertucco: Development of kinetic model and validation.
Viktor Hacker: Supervision, validation, project administration, funding acquisition.

Conflict of interest

The authors declare that they have no known competing financial interests or personal relationships that could have appeared to influence the work reported in this paper.

ORCID iDs

B Stoppacher https://orcid.org/0000-0002-6551-9597
V Hacker https://orcid.org/0000-0001-5956-7579

References

[1] Laura C *et al* IEA 2021 *Global Energy Review 2021* (https://doi.org/10.1787/90c8c125-en)
[2] Surendra K C, Takara D, Hashimoto A G and Khanal S K 2014 Biogas as a sustainable energy source for developing countries: opportunities and challenges *Renew. Sustain. Energy Rev.* **31** 846–59
[3] Wasajja H, Lindeboom R E F, van Lier J B and Aravind P V 2020 Techno-economic review of biogas cleaning technologies for small scale off-grid solid oxide fuel cell applications *Fuel Process. Technol.* **197** 106215
[4] Jablonski W S, Villano S M and Dean A M 2015 A comparison of H_2S, SO_2, and COS poisoning on Ni/YSZ and Ni/K_2O-$CaAl_2O_4$ during methane steam and dry reforming *Appl. Catal.* A **502** 399–409
[5] Staničić I, Andersson V, Hanning M, Mattisson T, Backman R and Leion H 2019 Combined manganese oxides as oxygen carriers for biomass combustion—ash interactions *Chem. Eng. Res. Des.* **149** 104–20
[6] Chiodo V, Maisano S, Zafarana G and Urbani F 2017 Effect of pollutants on biogas steam reforming *Int. J. Hydrog. Energy* **42** 1622–8
[7] Mancino G, Cimino S and Lisi L 2016 Sulphur poisoning of alumina supported Rh catalyst during dry reforming of methane *Catal. Today* **277** 126–32
[8] Argyle M D and Bartholomew C H 2015 Heterogeneous catalyst deactivation and regeneration: a review *Catalysts* **5** 145–269
[9] Bartholomew C H 2001 Mechanisms of catalyst deactivation *Appl. Catal.* A **212** 17–60
[10] Hacker V 2003 A novel process for stationary hydrogen production: the reformer sponge iron cycle (RESC) *J. Power Sources* **118** 311–4
[11] Bock S, Stoppacher B, Malli K, Lammer M and Hacker V 2021 Techno-economic analysis of fixed-bed chemical looping for decentralized, fuel-cell-grade hydrogen production coupled with a 3 MWth biogas digester *Energy Convers. Manage.* **250** 114801
[12] Appari S, Janardhanan V M, Bauri R, Jayanti S and Deutschmann O 2014 A detailed kinetic model for biogas steam reforming on Ni and catalyst deactivation due to sulfur poisoning *Appl. Catal.* A **471** 118–25
[13] Alstrup J R, Rostrup-Nielsen J R and Roen S 1981 High temperature hydrogen sulfide chemisorption on nickel catalysts *Appl. Catal.* **1** 303–14
[14] Sadooghi P and Rauch R 2015 Experimental and modeling study of hydrogen production from catalytic steam reforming of methane mixture with hydrogen sulfide *Int. J. Hydrog. Energy* **40** 10418–26
[15] Adánez-Rubio I, Abad A, Gayán P, García-Labiano F, de Diego L F and Adánez J 2014 The fate of sulphur in the Cu-based chemical looping with oxygen uncoupling (CLOU) process *Appl. Energy* **113** 1855–62
[16] Forero C R, Gayán P, García-Labiano F, de Diego L F, Abad A and Adánez J 2010 Effect of gas composition in chemical-looping combustion with copper-based oxygen carriers: fate of sulphur *Int. J. Greenh. Gas Control* **4** 762–70
[17] Wang B, Gao C, Wang W, Zhao H and Zheng C 2014 Sulfur evolution in chemical looping combustion of coal with $MnFe_2O_4$ oxygen carrier *J. Environ. Sci.* **26** 1062–70
[18] Pachler R F, Penthor S, Mayer K and Hofbauer H 2019 Fate of sulfur in chemical looping combustion of gaseous fuels using a perovskite oxygen carrier *Fuel* **241** 432–41
[19] Stoppacher B, Sterniczky T, Bock S and Hacker V 2022 On-site production of high-purity hydrogen from raw biogas with fixed-bed chemical looping *Energy Convers. Manage.* **268** 115971
[20] Fogler H S 2016 *Elements of Chemical Reaction Engineering* 5th edn (New York: Pearson)
[21] Halabi M H, de Croon M H J M, van der Schaaf J, Cobden P D and Schouten J C 2008 Modeling and analysis of autothermal reforming of methane to hydrogen in a fixed bed reformer *Chem. Eng. J.* **137** 568–78
[22] Xu J and Froment G F 1989 Methane steam reforming, methanation and water-gas shift: i. Intrinsic kinetics *AIChE J.* **35** 88–96
[23] Cipitì F, Barbera O, Briguglio N, Giacoppo G, Italiano C and Vita A 2016 Design of a biogas steam reforming reactor: a modelling and experimental approach *Int. J. Hydrog. Energy* **41** 11577–83
[24] Rostrup-Nielsen J R 1984 Sulfur-passivated nickel catalysts for carbon-free steam reforming of methane *J. Catal.* **85** 31–43
[25] Appari S, Janardhanan V M, Bauri R and Jayanti S 2014 Deactivation and regeneration of Ni catalyst during steam reforming of model biogas: an experimental investigation *Int. J. Hydrog. Energy* **39** 297–304
[26] Qi R, An L, Guo Y, Zhang R and Wang Z J 2022 *In situ* fabrication of ultrasmall Ni nanoparticles from $Ni(OH)_2$ precursors for efficient CO_2 reforming of methane *Ind. Eng. Chem. Res.* **61** 198–206
[27] Bai X, Xie G, Guo Y, Tian L, El-Hosainy H M, Awadallah A E, Ji S and Wang Z-J 2021 A highly active Ni catalyst supported on Mg-substituted $LaAlO_3$ for carbon dioxide reforming of methane *Catal. Today* **368** 78–85

[28] Rostrup-Nielsen J and Christiansen L 2011 *Concepts in Syngas Manufacture* 10th edn Catalytic Science (London: Imperial College Press)
[29] Ashrafi M, Pfeifer C, Pröll T and Hofbauer H 2008 Experimental study of model biogas catalytic steam reforming: 2. Impact of sulfur on the deactivation and regeneration of Ni-based catalysts *Energy Fuels* **22** 4190–5
[30] Yang X 2017 An experimental investigation on the deactivation and regeneration of a steam reforming catalyst *Renew. Energy* **112** 17–24
[31] Stoppacher B, Bock S, Malli K, Lammer M and Hacker V 2022 The influence of hydrogen sulfide contaminations on hydrogen production in chemical looping processes *Fuel* **307** 121677